Journal of Inorganic Biochemistry 203 (2020) 110929

Contents lists available at ScienceDirect

Journal of Inorganic Biochemistry

journal homepage: www.elsevier.com/locate/jinorgbio

Modified EDTA selectively recognized Cu^{2+} and its application in the disaggregation of β-amyloid-Cu (II)/Zn (II) aggregates

Renke Chang[1], Xiang Chen[1], Huijuan Yu, Guizhen Tan, Hongli Wen, Jianxin Huang, Zhifeng Hao*

School of Chemical Engineering and Light Industry, Guangdong University of Technology, Guangzhou 510006, PR China

ARTICLE INFO

Keywords:
Modified EDTA
Cu^{2+} recognition
β-Amyloid (Aβ)
Alzheimer's disease
Aβ-Cu (II)/Zn (II) aggregates
Disaggregation

ABSTRACT

The accumulation of the β-amyloid (Aβ) aggregates induced by Cu^{2+}/Zn^{2+} in conjunction with toxicity is closely related to Alzheimer's disease (AD). Herein, we intended to improve the efficiency and selectivity of traditional chelator ethylenediaminetetraacetic acid (EDTA) combined with a fluorescent group 4-aminosalicylic acid (4-ASA)to acquire a novel potential chelator 4,4′-((2,2′-(ethane-1,2-diylbis((carboxymethyl)azanediyl))bis(acetyl))bis(azanediyl))bis(2-hydroxybenzoic acid) (**EDTA-ASA**) capable of disaggregating Aβ-Cu(II)/ Zn(II) aggregates. **EDTA-ASA** combines 4-ASA as fluorophore and multidentate amino nitrogen, hydroxyl and carboxyl groups to chelate Cu^{2+} from Aβ-Cu (II) aggregates. The specific selectivity of **EDTA-ASA** towards Cu^{2+} in Tris-HCl buffer solution was investigated by fluorescence measurements. It exhibits high recognition towards Cu^{2+} with no significant interference of other competitive metal ions, which overcomes the deficiencies of EDTA. Importantly, the binding sites and binding mode for Cu^{2+} were clarified through DFT calculations. The thioflavin-T (ThT) fluorescence analyses and transmission electron microscopy (TEM) results have revealed **EDTA-ASA** exhibited an enhanced disaggregation capability on Aβ-Cu (II)/Zn (II) aggregates in comparison to EDTA. The Cu^{2+} chelating affinity was sufficient for **EDTA-ASA** to sequester Cu^{2+} from Aβ-Cu (II) aggregates.

1. Introduction

Alzheimer's disease (AD) is the most common form of dementia in the world and a devastating neurodegenerative disorder, it is incurable so far [1]. The predominant cause of AD is a heated discussion. Currently, though multiple factors mutually influence each other, the most prevailing hypothesis is still the amyloid cascade [2,3]. The amyloid cascade proposes amyloid-β (Aβ) aggregation as the leading cause of the disease. The misfolding of the extracellular Aβ accumulated in senile plaques (SP) has been recognized as the dominant hallmark of AD [4]. Aβ is a typical 39–43 residue polypeptide encompassing a C-terminal hydrophobic domain and an N-terminal hydrophilic sequence. Its interaction with Cu^{2+}, Zn^{2+} facilitates Aβ aggregation, Aβ misfolding and reactive oxygen species (ROS) production [5–7]. Especially, high millimolar concentrations range of Cu^{2+} and Zn^{2+} are found in SP [8]. Up to now, the treatment of AD faces the greatest challenges in that there are few competent therapeutic approaches to modulate related metal ions and disaggregate Aβ-Cu (II)/Zn (II) aggregates.

Metal chelators have been applied in AD therapy research due to their metal ion chelating ability and have been proven to be a critical approach [9–12]. In the past few decades, plenty of chelators for metal ions, especially for Cu^{2+} selective recognition, have been reported such as ethylenediaminetetraacetic acid (EDTA) [13], quinolines [14], clioquinol (CQ) [15a], 5,7-dichloro-2-((dimethylamino)methyl) 8-quinolinol (PBT-2) [16], calixarenes [17], curcumins [18], and rhodamines [19,20]. Potential regulation of Cu^{2+}-induced Aβ aggregation has been shown in vitro and in vivo by using these metal chelators. Several chelators including CQ and PBT2 have been employed in murine AD

Abbreviations: AD, Alzheimer's disease; Aβ, Amyloid-β; SP, Senile plaques; ROS, Reactive oxygen species; EDTA, Ethylenediaminetetraacetic acid; CQ, Clioquinol; PBT-2, 5,7-dichloro-2-((dimethylamino)methyl) 8-quinolinol; 4-ASA, 4-aminosalicylic acid; EDTA-ASA, 4,4′-((2,2′-(ethane-1,2-diylbis ((carboxymethyl)azanediyl))-bis(acetyl))bis(azanediyl))bis(2-hydroxybenzoic acid); PET, Photoinduced electron transfer; NMR, Nuclear magnetic resonance; ESI-MS, Electrospray ionization mass spectra; FT-IR, Fourier transform infrared; UV–vis, Ultraviolet-visible; TEM, Transmission electron microscope; EDTA-DA, 4-[2-(2,6-dioxomorpholin-4-yl) ethyl] morpholine-2,6-dione; Py, pyridine; DFT, Density functional theory; B3LYP, Becke-3-Lee-Yang-Parr; MOs, Molecular orbitals; HOMO, Highest Occupied Molecular Orbital; LOMO, Lowest Unoccupied Molecular Orbital; HFIP, 1,1,1,3,3,3-hexafluoro-2-propanol; ThT, Thioflavin T; CHEQ, Chelation-enhanced fluorescence quenching; ISC, Intersystem crossing; K_a, Binding association constant; B-H, equation Benesi-Hildebrand equation

* Corresponding author.
E-mail address: haozf@gdut.edu.cn (Z. Hao).

[1] These authors contributed equally to this work.

https://doi.org/10.1016/j.jinorgbio.2019.110929
Received 20 June 2019; Received in revised form 14 November 2019; Accepted 15 November 2019
Available online 23 November 2019
0162-0134/

models and AD patients. CQ was proved to be capable of dissolving Aβ deposits in transgenic mice and it can slow the cognitive decline associated with AD in some cases, and PBT2 could decrease the levels of Aβ in AD patients. Yet, all these metal chelators have not yielded promising results. The unpredictable side effects of these metal chelators, including drug-resistance and subacute myelo-optic neuropathy, limit their universal clinical applications. Besides, most of these chelators exhibited limited application due to problems such as complicated synthetic procedures, poor water solubility, and high interference by co-existing metal ions [21–24]. Therefore, bearing the above considerations in mind, the functional chelator designs are still novel, and useful methods. It is of great significance and necessary to develop a novel metal chelator which exhibits high selectivity towards Cu^{2+} in aqueous solution via a simply synthetic method.

Interestingly, the well-known chelator, EDTA, has attracted considerable attention in recent years [25–27]. Despite its limitations in clinical studies, its EDTA backbone inspires us to functionalize it further to improve its possible properties. We have started to construct a modified EDTA derivative as a functional metal chelator. 4-aminosalicylic acid (4-ASA) has been widely utilized for the treatment of inflammatory diseases since the 1940s [28–31]. ASA conjugates of EDTA were reported as promising anti-inflammatory prodrugs [32]. The compound 4-ASA possesses a fluorescent moiety which is useful for probing metal ions. Furthermore, 4-ASA conjugates of EDTA derivative as a chelator for selective recognition of Cu^{2+} in AD therapy has not been reported [33,34]. From the above, we have herein proposed to conjugate 4-ASA to EDTA with the amide linkage (-CONH) as a bridging unit to acquire the desired chelator, which will show water solubility improvement, strong fluorescence, and be capable for specific recognition of Cu^{2+} in aqueous solution.

We strategically designed and synthesized a modified EDTA derivative 4,4′-((2,2′-(ethane-1,2-diylbis ((carboxymethyl)azanediyl)) bis (acetyl)) bis(azanediyl))bis(2-hydroxybenzoic acid) (**EDTA-ASA**) (scheme. 1). It is based on EDTA as receptor and modified with 4-ASA as fluorophore. **EDTA-ASA** comprising both 4-ASA and EDTA-backbone group could provide excellent coordinating sites, such as electron-rich N (amino-nitrogen, -NH-) and O (hydroxyl and carboxyl groups, –OH, –COOH) atoms. Both the framework of EDTA and side cores of 4-ASA have the potential to chelate Cu^{2+}. **EDTA-ASA** presents a highly symmetrical structure, which is hoped to provide a special configuration and binding cavity for Cu^{2+}. In addition, the groups of –COOH and –OH on 4-ASA could increase the solubility in aqueous solution. The -CONH extends the distance between the two functional groups thereby adjusting the effect of photoinduced electron transfer (PET) of secondary amines of 4-ASA to EDTA group. Furthermore, the –COOH and the –OH group in **EDTA-ASA** may have electrostatic interactions and hydrogen bonds with the carbonyl groups of N-terminal residues at Aβ. Besides the chelating interaction with Cu^{2+}, **EDTA-ASA** is expected to have other synergistic effects to disaggregate the Cu (II)/Zn (II)-mediated Aβ aggregates. Collectively, **EDTA-ASA** is anticipated to have a wide potential application as potential chelator agents in the field of AD therapy.

2. Experimental section

2.1. Materials and methods

All chemical reagents (analytic grade or molecular biology grade) purchased commercially were available and can be used as is unless otherwise specified. The solutions of metal cations were performed from their corresponding salts, such as LiCl, NaCl, KCl, $MgCl_2{\cdot}6H_2O$, $CaCl_2{\cdot}4H_2O$, $AlCl_3{\cdot}6H_2O$, $BaCl_2$, $ZnCl_2$, $AgNO_3$, $MnCl_2{\cdot}4H_2O$, $Pb(NO_3)_2$, $CrCl_3{\cdot}6H_2O$, $CoCl_2{\cdot}6H_2O$, $NiCl_2{\cdot}6H_2O$, $HgCl_2$, and $CuCl_2{\cdot}3H_2O$. For the investigation of anions on the effect of recognition, the different water-soluble chloride, sulphate, nitrate, bromide, perchlorate, and acetate salts of copper ($CuCl_2$, $CuSO_4$, $Cu(NO_3)_2$, $CuBr_2$, $Cu(ClO_4)_2$, and $Cu(OAc)_2$) were used. The water used in this work is ultrapure water (18.2 MΩ cm) deionized by the Milli-Q system. $A\beta_{40}$ is the most predominant forms of Aβ in vivo. $A\beta_{40}$ peptide (free acid terminal) was commercially purchased from Sangon Biotech (Shanghai, China) and kept at −20 °C. The sequence of amino acid for the $A\beta_{40}$ is DAEFRHDSGYEVHHQKLVFFAEDVGSNKGAIIGLMVGGVV. The nuclear magnetic resonance (NMR) spectra were employed on Bruker AVANCE III HD 400 in D_2O. Electrospray ionization mass spectra (ESI-MS) were determined on a Shimadzu, Japan LCMS-2020 Liquid Chromatograph-Mass Spectrometer using methanol as a solvent. The Fourier transform infrared (FT-IR) spectra were determined ranging from 4000 to 400 cm^{-1} on a THEMOR-FILSHER iS50R instrument using KBr pellets.

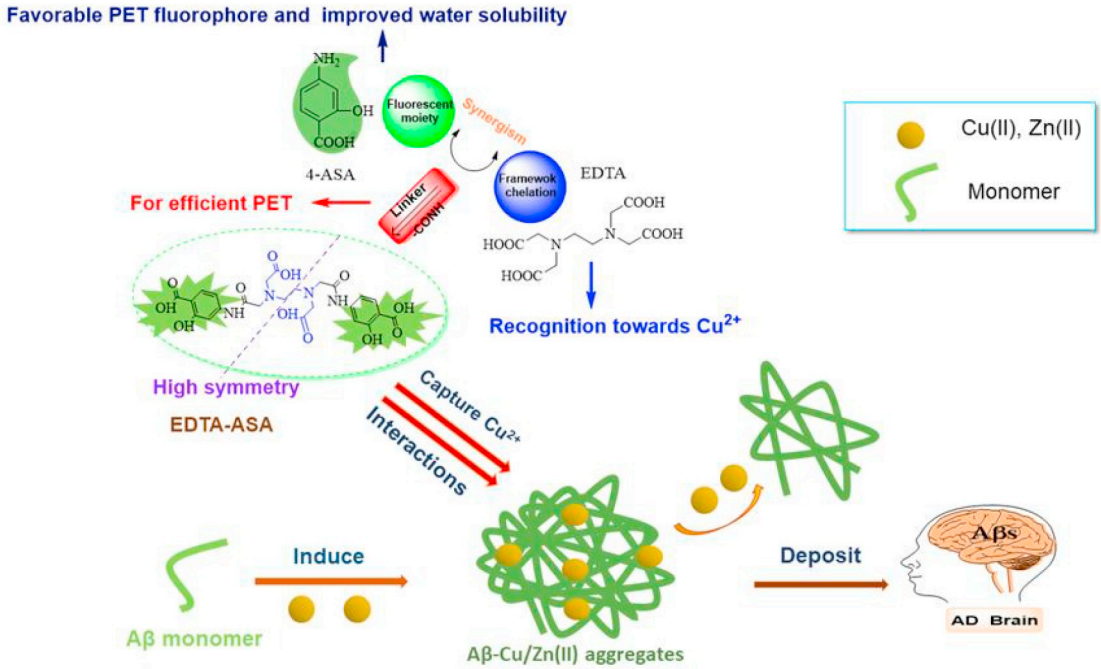

Scheme 1. Schematic illustration of the design strategy of **EDTA-ASA** and its disaggregation in Aβ-Cu (II)/ Zn (II) aggregates.

Ultraviolet-visible (UV–vis) spectra were measured on PerkinElmer Lambda 950 spectrophotometer. Fluorescence spectra were recorded on a HORIBA Jobin Yvon FluoroMax-4 Fluorescence Spectrometer. Both absorption and emission spectra were acquired at ambient temperature. All tests were performed in parallel three times, and data processing were expressed as the mean and standard deviation. Transmission electron microscope (TEM) analysis was performed on the Shimadzu, Japan HT7700.

2.2. Synthesis of 4,4′-((2,2′-(ethane-1,2-diylbis((carboxymethyl) azanediyl)) bis(acetyl))bis(azanediyl))bis(2-hydroxybenzoic acid) (EDTA-ASA)

The 4-[2-(2,6-dioxomorpholin-4-yl) ethyl] morpholine-2,6-dione (EDTA-DA) (2.56 g (0.01 mol)), and 4-ASA (3.06 g (0.02 mol)) were combined in 20 mL DMF under nitrogen atmosphere. 8 mL of pyridine (Py) was sequentially added dropwise to the mixed solution. The solid was completely dissolved for 15 min, and the reaction was stirred at 30 °C for 24 h. After the reaction was completed, the reaction mixture was poured into $CHCl_3$ to give a white precipitate. The obtained product was collected by filtration under vacuum and washed with anhydrous ethanol. After vacuum drying at 60 °C for 5 h, a white powder was obtained. This white powder was dissolved in an appropriate amount of NaOH and then was followed by acidification by adding 0.1 M HCl dropwise. The pure white precipitate of **EDTA-ASA** was finally obtained by vacuum filtration in a yield of 92%.

2.3. UV–vis spectra and fluorescence measurements of EDTA-ASA with metal ions

The metal ions stock solution was prepared in ultrapure water using the corresponding metal salts. This stock solution of **EDTA-ASA** was prepared and diluted to desired concentration with Tris-HCl buffer solution (10 mM, pH 7.4). Both UV–vis spectrum and fluorescence emission spectrum were performed according to the following procedures. In the UV–visible experiment, the **EDTA-ASA** solution was placed in a quartz cell with an optical path of 1.0 cm to achieve an absorption spectrum. For emission experiment, the solution of **EDTA-ASA** 2000 μL was filled in a quartz cell with 1.0 cm optical path, the solution of different metal ions was added and gradually mixed with a micropipette for 3 min. The fluorescence titration experiment was measured by mixing **EDTA-ASA** with a different molar ratio of Cu^{2+} solution.

2.4. Computational details

Density functional theory (DFT) theoretical calculation was employed to investigate the binding mode between **EDTA-ASA** and Cu^{2+}, based on the 6-31G* in conjuration with Becke-3-Lee-Yang-Parr (B3LYP) basis set [35–37]. The 6-31G* basis set was selected for non-metallic elements such as the C, H, O, and N atoms; the SDD basis set was for the Cu atom. The structures of **EDTA-ASA** and **EDTA-ASA**-Cu complex were optimized with the DFT calculations. Vibrational frequencies of the structure have been analyzed to confirm the minima optimized structures. All theoretical calculations were accomplished on the Gaussian 09 programs. The molecular orbitals (MOs) of **EDTA-ASA** and **EDTA-ASA**-Cu were visualized and plotted with the Gauss-View program.

2.5. HFIP treatment of Aβ40

The initial powder of $A\beta_{40}$ was dissolved in cooled 1,1,1,3,3,3-hexafluoro-2-propanol (HFIP) with constant agitation for 6 h to obtain a homogeneous $A\beta_{40}$ monomeric solution. The solution was blowing with argon gas stream to evaporate the HFIP. The obtained thin white films of the $A\beta_{40}$ monomer were stored at −20 °C. Monomeric films were dissolved in DMSO with agitation to acquire a final concentration of 1.0 mg·mL^{-1}. The stock solution of $A\beta_{40}$ was diluted with Tris-HCl buffer solution (10 mM, pH 7.4) to desired concentrations for the following experimental.

2.6. Thioflavin T (ThT) fluorescence study

ThT fluorescence investigations were employed with a fluorescence spectrometer. In the inhibition studies, freshly prepared $A\beta_{40}$ (25 μM) in the presence or absence of Cu (II) or Zn (II) (25 μM) was mixed with or without EDTA and **EDTA-ASA** (25 μM) and incubated at 37 °C with constant agitation for 24 h. In the disaggregation studies, metal-free and metal treated $A\beta_{40}$ (25 μM) aggregates were generated by incubating mixtures of freshly prepared $A\beta_{40}$ (25 μM) in the presence or absence of Cu (II) or Zn(II) (25 μM) at 37 °C with agitation. After 24 h, the samples were treated with EDTA and **EDTA-ASA** (25 μM) and incubated for another 24 h. After incubation, all of the samples were treated with ThT for the following ThT studies (λ_{ex} = 404 nm, λ_{em} = 487 nm).

2.7. Transmission electron microscopy (TEM)

Samples for TEM were prepared by the following steps. The glow-discharged grid (Formar/Carbon 300-mesh, Electron Microscopy Sciences) was treated with the corresponding $A\beta_{40}$, and $A\beta_{40}$-Cu (II)/Zn (II) aggregates samples (25 μM, 5 μL) for 2 min at ambient temperature. Excess samples were removed with filter paper and then washed twice with ultrapure water. Each grid dried for 30 min at room temperature. Images from each sample were captured by a Shimadzu, Japan HT7700 (40–120 kV, Image rotation: maximum range X1000-X40000 magnification).

3. Results and discussion

3.1. Synthesis and general characterization of EDTA-ASA

EDTA-ASA was synthesized in 92% yield via one-step reaction from the starting materials EDTA-DA and 4-ASA respectively (as illustrated in Scheme. 2). The structure of **EDTA-ASA** was well characterized by ESI-MS, FT-IR, ^{1}H NMR, and ^{13}C NMR. All data match well with the corresponding structure.

3.2. The spectroscopic studies of EDTA-ASA towards Cu^{2+} recognition

In the UV–vis spectra, **EDTA-ASA** showed two main absorption bands located at 260 nm and 302 nm in Tris-HCl buffer solution (Fig. S5, ESI†). The UV–vis spectrum of 4-ASA exhibited a similar major absorption band at 263 nm and 298 nm in Tris-HCl buffer solution (Fig. S6, ESI†). The maximum absorbance band located at 260 nm corresponds to benzene ring π-π* transition and the band centered at 302 nm is attributed to the charge transition from benzene ring to an amino group. Therefore, we choose the band centered at 260 nm as the excitation wavelength in the subsequent fluorescent studies.

To investigate the selectivity of **EDTA-ASA**, the tested metal ions including Cu^{2+}, Zn^{2+}, Li^{+}, Na^{+}, K^{+}, Mg^{2+}, Ca^{2+}, Al^{3+}, Ba^{2+}, Ag^{+}, Mn^{2+}, Pb^{2+}, Cr^{3+}, Co^{2+}, Ni^{2+} and Hg^{2+} were employed in our study. Fig. 1 shows the fluorescence emission spectra of **EDTA-ASA** in the

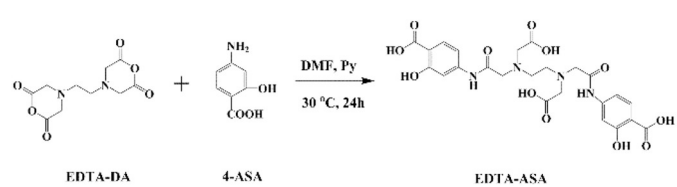

Scheme 2. The synthesis procedure of **EDTA-ASA**

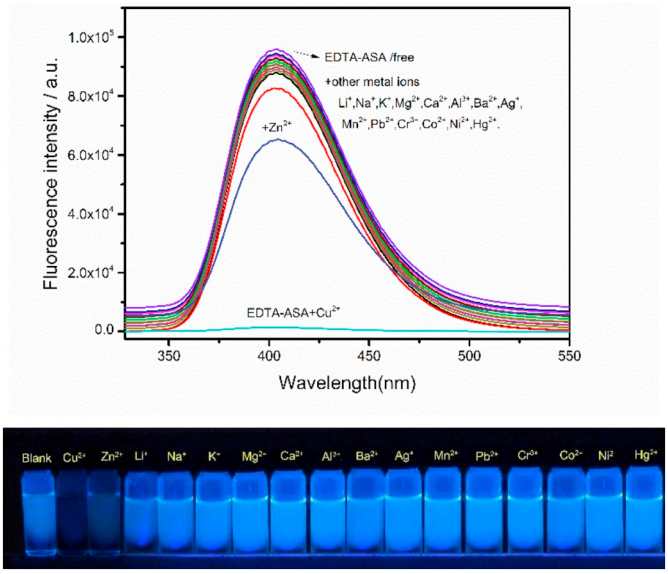

Fig. 1. Fluorescence spectrum of **EDTA-ASA** (10 μM) on addition of different metal ions (10 μM) of Cu^{2+}, Zn^{2+}, Li^{+}, Na^{+}, K^{+}, Mg^{2+}, Ca^{2+}, Al^{3+}, Ba^{2+}, Ag^{+}, Mn^{2+}, Pb^{2+}, Cr^{3+}, Co^{2+}, Ni^{2+} and Hg^{2+} in Tris-HCl buffer solution (10 mM, pH 7.4). Image: Selective fluorescent response of **EDTA-ASA** in the presence of metal ions (under UV light).

presence of 1.0 equal different metal ions. Collectively, **EDTA-ASA** alone had relatively strong fluorescence centered at near 403 nm in Tris-HCl buffer solution. Upon addition with 1.0 equal Cu^{2+}, while, the fluorescence at 403 nm was almost wholly quenched. The fluorescence changed from "on" to "off." In contrast, the other metal ions including Zn^{2+} failed to show any dramatic fluorescence change in fluorescence behavior of **EDTA-ASA**. The UV–vis spectra of EDTA-ASA on addition of different metal ions in Tris-HCl buffer solution were also employed (Fig. S7, ESI†). For comparison purpose, we also investigated the fluorescence properties of control compound 4-ASA in Tris-HCl buffer solution. A negligible response of 4-ASA was observed towards all the tested metal ions (Fig. S8, ESI†). Therefore, the results confirmed that **EDTA-ASA** exhibited good selectivity and displayed a dynamic "on-off" behavior towards Cu^{2+} in Tris-HCl buffer solution.

Notably, the efficient quenching of fluorescence indicated that **EDTA-ASA** showed a specific response to Cu^{2+}. Before coordination with Cu^{2+}, **EDTA-ASA** have strong fluorescence. However, when **EDTA-ASA** was coordinated with Cu^{2+}, the fluorescence is quenched, which is probably due to the formation of a non-fluorescent complex **EDTA-ASA**-Cu. This "on-off" switching could be explained with chelation-enhanced fluorescence quenching (CHEQ) effect and PET-enhanced process [38–40]. These metal ions differ too much in many ways such as the orbital shape, electron density, size of the metal ion, and they can establish different coordination interactions. The metal ions that failed to cause a significant change in fluorescence intensity may be due to the inappropriate coordination conformation and unsuitable ion radius. This phenomenon is following the case of d^9 Cu (II), it is the highest in the Irving-Williams series [41]. Moreover, due to the Jahn-Teller effect, the complex **EDTA-ASA**-Cu has higher stability [42]. Furthermore, Cu^{2+} is paramagnetic with an empty shell, the intrinsic paramagnetic nature of Cu^{2+} from spin-orbit coupling could actively quench the emission of a nearby fluorophore via non-radiative intersystem crossing (ISC) transition process [43,44].

The fluorescence titration investigations were used to explore the response properties of **EDTA-ASA** to Cu^{2+}. As is presented in Fig. 2(a), **EDTA-ASA** displayed strong fluorescence at 403 nm. Upon adding various molar of Cu^{2+} (0–1 equal) into **EDTA-ASA**, the fluorescence intensity gradually decreased, and the fluorescence intensity nearly remains unchanged even 1.0 equal Cu^{2+} was added. The results indicated the formation of 1:1 chelation ratio of **EDTA-ASA** and Cu^{2+}. The 1:1 binding mode between **EDTA-ASA** and Cu^{2+} was also established using Job's plot methods. The fluorescence emission intensity got a minimum when the molar ratio fraction was 0.5, which further verified a 1:1 stoichiometry of **EDTA-ASA** and Cu^{2+}. Cu^{2+} may be chelated at the N (-NH-, amino-nitrogen) and O (-COOH, carboxyl group) atoms of **EDTA-ASA** to satisfy the need for saturated 1:1 coordination by forming stable **EDTA-ASA**-Cu complex. Theoretical calculations based on DFT principles were employed to better understand the phenomenon of fluorescence quenching and the chelation interaction between **EDTA-ASA** and Cu^{2+} in the following discussions.

The binding association constant (K_a) is used to evaluate the stability of interaction between the chelator and metal ions together in a solution. We adopted the Benesi-Hildebrand eq. (B–H equation) to determine the K_a of **EDTA-ASA** and Cu^{2+} in Tris-HCl buffer solution [45]. There is a great linear relationship with the R^2 value of 0.9984 in Fig. 2(b). The K_a value was counted as 6.852×10^7 M^{-1} for **EDTA-ASA**-Cu complex, indicating a robust binding association between **EDTA-ASA** and Cu^{2+}. Moreover, the **EDTA-ASA**-Zn complex showed the same 1:1 stoichiometry, and the K_a was calculated to be 9.765×10^5 M^{-1}, which is far below that of **EDTA-ASA**-Cu complex (Fig. S9-S11, ESI†).

Competition experiments study further assessed the specificity of **EDTA-ASA** for Cu^{2+}. as shown in Fig. 3(a), there was almost no significant decrease in fluorescence intensity when **EDTA-ASA** was treated with 1 equal of other metal ions (Zn^{2+}, Li^{+}, Na^{+}, K^{+}, Mg^{2+}, Ca^{2+}, Al^{3+}, Ba^{2+}, Ag^{+}, Mn^{2+}, Pb^{2+}, Cr^{3+}, Co^{2+}, Ni^{2+}, and Hg^{2+}). However, upon addition of another 1 equal Cu^{2+} to the mixed solution of **EDTA-ASA** with other metal ions, an apparent fluorescence quenching was noticed. It was apparent that the quenching of fluorescence aroused by the mixture of Cu^{2+} with other metal ions was almost the same as that induced by Cu^{2+} only. As shown in Fig. 3(b), after **EDTA-ASA** was treated with of 1 equiv. Cu^{2+}, other excess 10 equiv. of competitive metal ions were added, there is almost no interference in fluorescence signal. Therefore, these consequences demonstrated that other common competitive metal ions do not significantly influence the recognition of **EDTA-ASA** for Cu^{2+}, which confirms that **EDTA-ASA** behaves high selectivity for Cu^{2+} in Tris-HCl buffer solution.

The fluorescence emission spectra of **EDTA-ASA** with different counter anions (SO_4^{2-}, Cl^{-}, NO_3^{-}, Br^{-}, ClO_4^{-}, and OAc^{-}) was investigated to determine the influence of interference anions on the recognition efficiency. This result illustrated that these anions had almost no interference with the recognition of Cu^{2+} (Fig. S12, ESI†). It is the chelation of Cu^{2+} and **EDTA-ASA** that leads to the efficient fluorescence quenching of **EDTA-ASA**, these anions exhibit no distinct effect on the recognition selectivity.

The reversibility of the fluorescence response process of **EDTA-ASA** towards Cu^{2+} was also explored with EDTA. After addition of excess EDTA to the **EDTA-ASA** and Cu^{2+} mixed solution, the fluorescence returned to the original fluorescence of **EDTA-ASA**, which strongly reveals that the Cu^{2+} recognition is a reversible chelation process (Fig. S13, S14, ESI†). These results may be connected with the different K_a between the chelators and Cu^{2+}. Tough its binding affinity of Cu^{2+} with **EDTA-ASA** (**EDTA-ASA**-Cu, $K_a = 6.852 \times 10^7$ M^{-1}, namely lg $K_a = 7.84$) is not as good as EDTA (EDTA-Cu, namely lg $K_a = 18.7$), it exhibits a high selectivity towards Cu^{2+} with much higher efficiency than EDTA.

It is well known that the stability of the metal chelator is of significance for further practical application. Thus, the interrelationship between the fluorescence of **EDTA-ASA** and pH variation was investigated to confirm the optimum pH range in application. When pH is in the range of 2–4, the fluorescence intensity of the fluorescence spectrum is nearly zero (Fig. S15, ESI†). This is probably due to the weak solubility of **EDTA-ASA** in Tris-HCl buffer solution. The fluorescence intensity of **EDTA-ASA** increased moderately with the change of pH from 4 to 7 and maintained relative stability in the pH range of

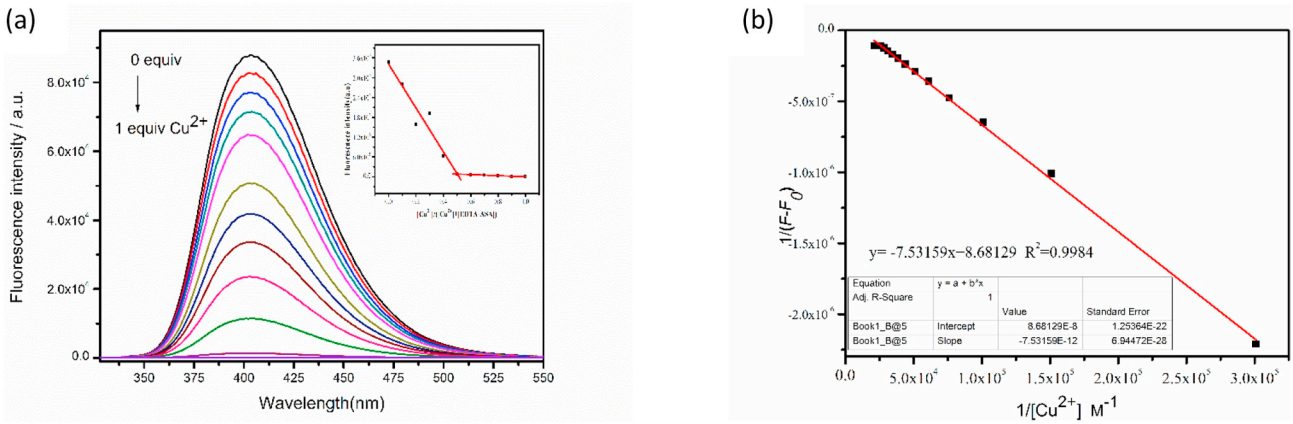

Fig. 2. (a) Fluorescence spectra of **EDTA-ASA** with addition of various concentrations of Cu^{2+} (0–1 equal, the total concentration of **EDTA-ASA** and Cu^{2+} was 10 μM) in Tris-HCl buffer solution (10 mM, pH 7.4). Inset: the drawing is Job's plot of the complexation between the **EDTA-ASA** and Cu^{2+}. **(b)** Benesi-Hildebrand plot of **EDTA-ASA**-Cu complex in Tris-HCl buffer solution (10 mM, pH 7.4).

7–12, which is ascribed to the protonation and deprotonation of **EDTA-ASA** with multiple hydroxyl and amino groups.

Furthermore, the influence of the time on the fluorescence intensity of **EDTA-ASA** over the range from 0 to 72 h in Tris-HCl buffer solution was also evaluated. The results reveal that the fluorescence intensity barely changes in a 10% range within a period of time (Fig. S16, ESI†). Namely, the aqueous solution of **EDTA-ASA** and its fluorescence properties are relatively stable, which means it may overcome the physiological fluctuations and maintain expected performances.

3.3. Theoretical calculations

The outstanding performances of **EDTA-ASA** in the recognition of Cu^{2+} drive us to explore its binding mode. Based on the results of fluorescence titration experiments and Job's plot, we hereby got the optimized energy-minimized structures of **EDTA-ASA** and **EDTA-ASA**-Cu by DFT optimization simulation calculations (as shown in Fig. 4). Fig. S17, and Fig. S18 ESI† illustrated the energy optimization curves under the best binding mode between **EDTA-ASA** and Cu^{2+}. The optimized structure of **EDTA-ASA** showed that it had a symmetrical plane containing the fluorophore and the receptor. The Cu^{2+} coordination changes the conformational states of **EDTA-ASA**. The structure of **EDTA-ASA**-Cu displays that the Cu^{2+} binds to **EDTA-ASA** at the amino nitrogen atoms and the carboxyl groups of core framework EDTA through four coordination sites. And, the Cu − O bond lengths are 2.03991 Å and 2.13863 Å, the Cu − N bond lengths are 2.03111 Å and 2.03989 Å, respectively, which means a strong coordination bond interaction between **EDTA-ASA** and Cu^{2+}. The coordination distances are suitable for Cu^{2+} binding and utilized exclusively for Cu^{2+}. These data indicated that the structure of **EDTA-ASA** could effectively provide

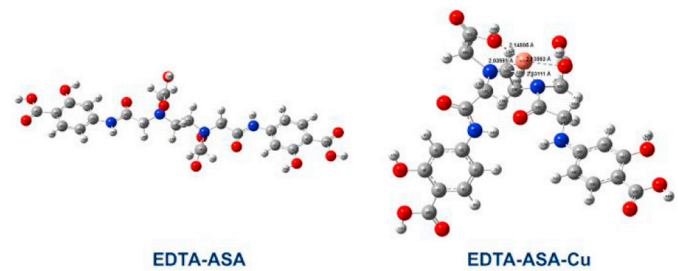

Fig. 4. Optimized energy-minimized structure of **EDTA-ASA** and **EDTA-ASA**-Cu (C, N, O H, and Cu atom are represented as grey, blue, red, white-grey, and orange respectively).

appropriate space to accommodate the Cu^{2+} and a cavity-like structure was generated to tether Cu^{2+} successfully.

In addition to the localization of the MOs (molecular orbital), E_{HOMO}, E_{LUMO}, and the HOMO (the highest occupied molecular orbital)-LUMO (the lowest unoccupied molecular orbital) band gap ($\Delta E = E_{LOMO}$-E_{HOMO}) are commonly used parameters to interpret the electronic properties and chelation behavior. Therefore, the orbital energies and the spatial electronic cloud distributions of the HOMO and the LUMO of **EDTA-ASA** and **EDTA-ASA**-Cu complexes were shown in Fig. 5. The HOMO of **EDTA-ASA** is primarily delocalized on the fluorophore 4-ASA part, the LUMO is the same as the distribution of HOMO. There is no electron transfer, And the PET process is prohibited, **EDTA-ASA** showed fluorescence. However, when **EDTA-ASA** is converted to **EDTA-ASA**-Cu after coordinating with Cu^{2+}, the HOMO of **EDTA-ASA**-Cu is mostly delocalized on the Cu^{2+} and nearby EDTA part, while the LUMO is distributed on the fluorophore 4-ASA part. Under this

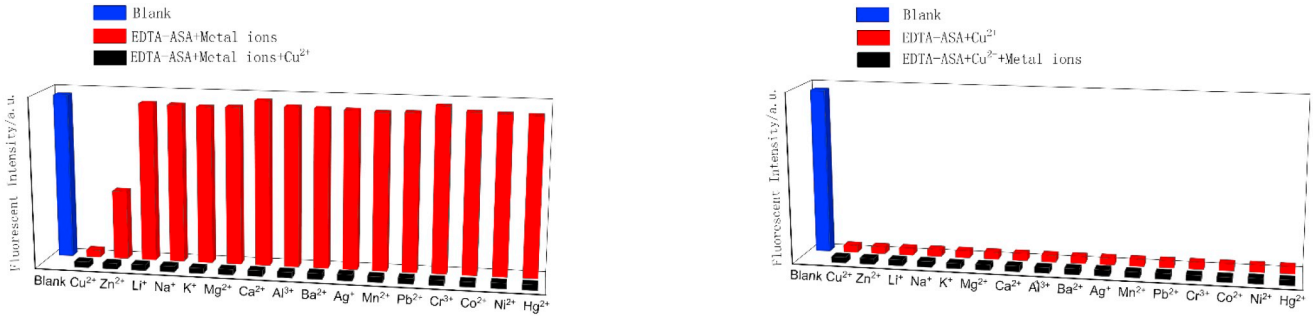

Fig. 3. (a) The fluorescence intensity at 403 nm of **EDTA-ASA** (10 μM) with metal ions in Tris-HCl buffer solution (10 mM, pH 7.4) and then with addition of equal molar of Cu^{2+}. **(b)** the fluorescence intensity at 403 nm of **EDTA-ASA** (10 μM) with the addition of equal molar of Cu^{2+} and then addition of excess 10 equiv. of other metal ions in Tris-HCl buffer solution (10 mM, pH 7.4).

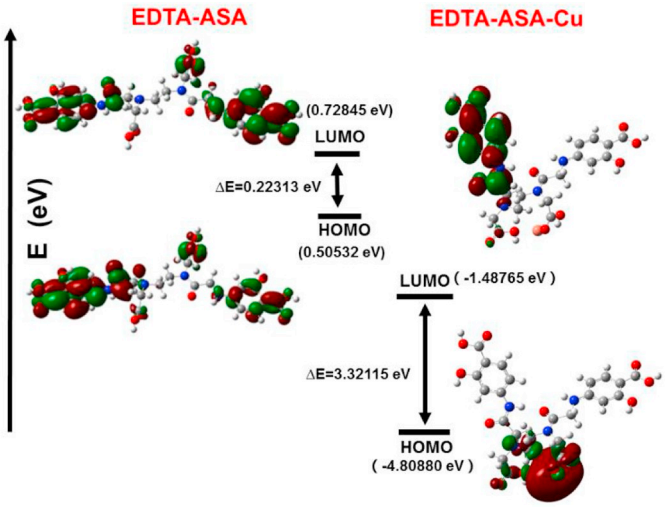

Fig. 5. Optimized frontier molecular orbital profiles for **EDTA-ASA** and its complex **EDTA-ASA**-Cu based on DFT (B3LYP/6-31G* set) calculation.

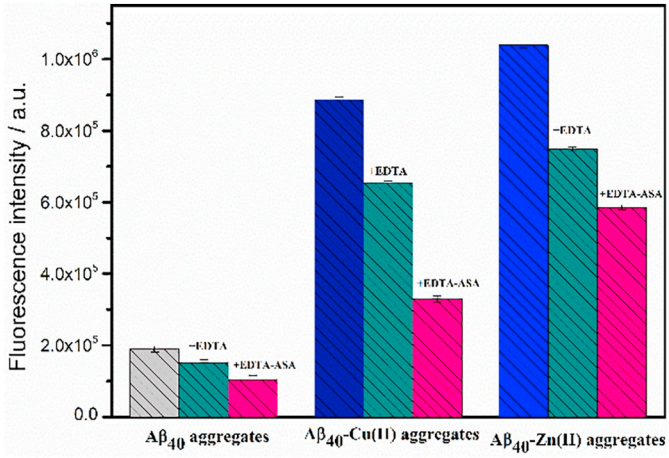

Fig. 6. The disaggregation of **EDTA-ASA** (Pink) and EDTA (Cyan) on corresponding $A\beta_{40}$ and $A\beta_{40}$-Cu (II)/Zn (II) aggregates in Tris-HCl buffer solution (10 mM, pH 7.4, λ_{ex} 440 nm, λ_{em} 487 nm,) were monitored by ThT fluorescence assay.

circumstance, this corresponds to the electron cloud distribution of the PET-enhanced process between the receptor and the fluorophore 4-ASA.

The ΔE between HOMO and LUMO of **EDTA-ASA** and **EDTA-ASA**-Cu was calculated as 0.22313 eV and 3.32115 eV, respectively. The ΔE between HOMO and LUMO of the **EDTA-ASA**-Cu complex had increased 3.09802 eV as compared to that of **EDTA-ASA**. Moreover, the geometry energy of **EDTA-ASA**-Cu was lower than EDTA-ASA (Fig. S17, Fig. S18, Table 1, ESI†). Therefore, the conversion of **EDTA-ASA** to **EDTA-ASA**-Cu becomes more accessible to form a stable **EDTA-ASA**-Cu complex by broadening the energy gap between HOMO and LUMO, which is also in accordance with Fang, Kim, Anand, and Hou's researches [46–49].

*3.4. Potential application of **EDTA-ASA** in disaggregating $A\beta_{40}$-Cu (II)/Zn (II) aggregates*

The ThT fluorescence study was explored to evaluate the ability of **EDTA-ASA** to inhibit and disaggregate Cu^{2+}/Zn^{2+}-induced $A\beta_{40}$ aggregates ($A\beta_{40}$-Cu (II)/Zn (II) aggregates). ThT is a benzothiazole fluorescent dye with a high affinity for β-sheet amyloid fibers, and it can be utilized to quantify the β-sheet content of Aβ aggregates [50]. As is clearly shown in Fig. S19-S21 ESI†, there's no fluorescence signal of the ThT in the fresh $A\beta_{40}$ solution. The solution of self-aggregated $A\beta_{40}$ sample only developed a limited increase in fluorescence intensity. In contrast, in the presence of Cu^{2+}/Zn^{2+}, there is a significant increase of approximately more than 4-fold in fluorescence signal, compared with the self-aggregated $A\beta_{40}$ aggregates, which suggest that Cu^{2+}/Zn^{2+} could induce the aggregation of $A\beta_{40}$ and the generation of the β-sheet structure. Although precise interaction mechanism of the Cu^{2+}/Zn^{2+} with $A\beta_{40}$ is still unclear, it is generally conjectured that these may result from the electrostatic and chelating interactions between Cu^{2+}/Zn^{2+} and $A\beta_{40}$. It is generally assumed that the Cu^{2+} can coordinate with $A\beta_{40}$ at N-terminal residues, such as His6, His13, His14, and thereby promote the aggregation of $A\beta_{40}$. Likewise, $A\beta_{40}$ could form a 1: 1 complex with Zn^{2+} [4,5,51]. When **EDTA-ASA** was added to the sample of $A\beta_{40}$-Cu (II)/Zn (II) aggregates, a decline in fluorescence was observed, which indicated that **EDTA-ASA** could inhibit the Cu^{2+}/Zn^{2+}-induced $A\beta_{40}$ aggregation. Moreover, **EDTA-ASA** also disaggregate $A\beta_{40}$-Cu (II)/Zn (II) aggregates. It is worth noted that the ability of **EDTA-ASA** to depolymerize $A\beta_{40}$-Cu (II)/Zn (II) aggregates is much stronger than the ability to inhibit aggregation, so **EDTA-ASA** was evaluated for its disaggregation capacity on self-induced $A\beta_{40}$, and Cu^{2+}/Zn^{2+}-induced $A\beta_{40}$ aggregates in subsequent investigations.

Table 1
The disaggregation results of **EDTA-ASA** and EDTA on corresponding $A\beta_{40}$ and $A\beta_{40}$-Cu (II)/Zn (II) aggregates.

Samples	DR[a] (%)	
	EDTA	EDTA-ASA
$A\beta_{40}$ aggregates	19.60 ± 0.23	44.20 ± 0.31
$A\beta_{40}$-Cu (II) aggregates	26.20 ± 0.21	62.20 ± 0.36
$A\beta_{40}$ − Zn (II) aggregates	8.20 ± 0.27	32.30 ± 0.33

DR[a] stands for disaggregation rate.

As shown in Fig. 6, the depolymerization rate of **EDTA-ASA** for $A\beta_{40}$-Cu (II) aggregates was 62.20%, which is 1.37-fold more effective than EDTA. EDTA, a natural product that is known to disaggregate Aβ-M (II) aggregates, was used as the reference compound [52]. We found that EDTA disaggregate $A\beta_{40}$-Cu (II) aggregates by a percentage similar to previous reports. (26.22% vs 24.50% disaggregation). **EDTA-ASA** was more effective at dissolving $A\beta_{40}$-Cu (II) aggregates compared with the control EDTA. Moreover, the consequence of **EDTA-ASA** to depolymerize in $A\beta_{40}$-Zn (II) aggregates is not as good as that of $A\beta_{40}$-Cu (II) aggregates. The ThT disaggregation results of **EDTA-ASA** and EDTA on the corresponding $A\beta_{40}$ aggregates are listed clearly in Table. 1.

TEM was exerted to directly study the morphology of corresponding $A\beta_{40}$ aggregates and visualize the disassembly effect of **EDTA-ASA**. As shown in Fig. 7, regular linear fibers morphology and little-fibrillary aggregates were detected in the samples of the self-aggregated $A\beta_{40}$, Cu^{2+}-induced $A\beta_{40}$ formed a denser aggregate than that of self-aggregated $A\beta_{40}$, larger aggregates were observed in Zn^{2+}-induced $A\beta_{40}$ aggregates. In the presence of **EDTA-ASA**, the large $A\beta_{40}$-Cu (II) aggregates were broken down into much smaller amorphous aggregates compared with the EDTA. The morphology of $A\beta_{40}$ −Cu (II) aggregates became smaller, and the structure was looser. All these findings are consistent with the above ThT fluorescent analysis. Consequently, it is assumed that the collapse of the $A\beta_{40}$-Cu (II) aggregates is mainly due to the capability of **EDTA-ASA** to chelate Cu^{2+}, and thus loosening the interactions of Cu^{2+} with the $A\beta_{40}$. At pH 7.4, the logarithm of the K_a of $A\beta_{40}$ for Cu^{2+} (lgK_a [Cu^{2+}-Aβ] = 5.80) is 5.80 [53]. This value is much lower compared with the affinity of **EDTA-ASA** for Cu^{2+} that has been obtained in the above discussions, (lgK_a [Cu^{2+}-EDTA-ASA] =7.84). Indeed, the affinity of **EDTA-ASA** to Cu^{2+} is greater than that of $A\beta_{40}$ (lgK_a [Cu^{2+}-Aβ] = 5.80, lgK_a [Cu^{2+}-EDTA-ASA] =7.84). Consequently, **EDTA-ASA** can extract Cu^{2+} complexed by $A\beta_{40}$ aggregates, resulting in the disassembly of the $A\beta_{40}$-Cu (II) aggregates. Also, the

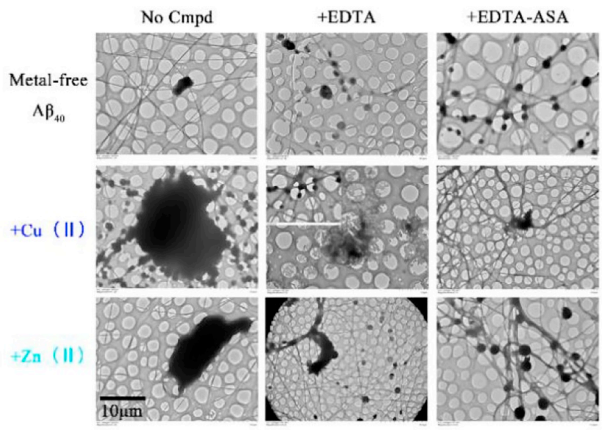

Fig. 7. Morphologies of the $A\beta_{40}$ aggregates after treatment with EDTA and **EDTA-ASA** as observed using TEM (scale bar 10 μm).

disaggregation ability of **EDTA-ASA** to $A\beta_{40}$-Cu (II) aggregates depends not only on the binding affinity of the **EDTA-ASA** to Cu^{2+}. The interactions of the electrostatic, hydrophilic, and hydrogen bonds of the **EDTA-ASA** with $A\beta_{40}$ aggregates are also possible [54,55], since the **EDTA-ASA** also disassembled $A\beta_{40}$ aggregates containing no Cu^{2+}/Zn^{2+}. In summary, **EDTA-ASA** has the potential to regulate dissociation of $A\beta_{40}$-Cu (II) aggregates perhaps by capturing aggregates containing Cu^{2+} and interacting with $A\beta_{40}$ aggregates.

4. Conclusion

In conclusion, the high selectivity for Cu^{2+} and disaggregation of $A\beta_{40}$-Cu (II)/Zn (II) aggregates have been achieved by developing a novel metal chelator **EDTA-ASA** based on EDTA as receptor and modified with 4-ASA as fluorophore. The **EDTA-ASA** exhibited exclusive selectivity towards Cu^{2+} and was not affected by other competitive metal ions in Tris-HCl buffer solution. Besides, **EDTA-ASA** displayed a dynamic "On-Off" response to Cu^{2+} owning to the CHEQ and PET process. The Job plot indicated that **EDTA-ASA** bound with Cu^{2+} in a 1:1 stoichiometry and the K_a was $6.852 \times 10^7\ M^{-1}$. DFT calculations provided an optimized structure of **EDTA-ASA**-Cu and further confirmed the 1:1 binding mode between **EDTA-ASA** and Cu^{2+} in a cavity-like structure. Thus, it can capture Cu^{2+} from $A\beta_{40}$-Cu (II) aggregates effectively. The findings indicate that this simple, practicable, designed chelator **EDTA-ASA** has good potential for the recognition for Cu^{2+} in disaggregating $A\beta_{40}$-Cu (II) aggregates. All these investigations propose a novel strategy for chelator design by introducing additional function group and open an avenue for promising exploration of more AD treatment chelators.

Declaration of competing interest

The authors declare that they have no known competing financial interests or personal relationships that could have appeared to influence the work reported in this paper.

Acknowledgments

We thank so much for the Special Fund of Guangdong Province Project for Applied Science and Technology Research and Development (Grant No: 2016B090930004) supported the work.

Appendix A. Supplementary data

Supplementary data to this article can be found online at https://doi.org/10.1016/j.jinorgbio.2019.110929.

References

[1] Alzheimer's Dement. 13 (2017) 325–373.
[2] J.A. Hardy, G.A. Higgins, Science 256 (1992) 184–186.
[3] F. Panza, M. Lozupone, D. Seripa, B.P. Imbimbo, Ann Neurol. 85 (2019) 303–315.
[4] J. Hardy, D. Allsop, Trends Pharmacol scI. 12 (1991) 383–388.
[5] G.F. Chen, T.H. Xu, Y. Yan, Y.R. Zhou, Y. Jiang, K. Melcher, H.E. Xu, Acta Pharmacol Sin. 38 (2017) 1205–1235.
[6] V. Lanza, D. Milardi, G. Di Natale, G. Pappalardo, Curr Med Chem. 25 (2018) 525–539.
[7] J.A. Duce, A.I. Bush, Prog Neurobiol. 92 (2010) 1–18.
[8] S. Jones, X. Zhang, D.W. Parsons, J.C.H. Lin, R.J. Leary, P. Angenendt, P. Mankoo, H. Carter, H. Kamiyama, A. Jimeno, S.M. Hong, B. Fu, M.T. Lin, E.S. Calhoun, M. Kamiyama, K. Walter, T. Nikolskaya, Y. Nikolsky, J. Hartigan, D.R. Smith, M. Hidalgo, S.D. Leach, A.P. Klein, E.M. Jaffee, M. Goggins, A. Maitra, C. Iacobuzio-Donahue, J.R. Eshleman, S.E. Kern, R.H. Hruban, R. Karchin, N. Papadopoulos, G. Parmigiani, B. Vogelstein, V.E. Velculescu, K.W. Kinzler, Science. 321 (2008) 1801–1806.
[9] A. Gnjec, J.A. Fonte, C. Atwood, R.N. Martins, Front Biosci. 7 (2002) 1016–1023.
[10] H. Zheng, L.M. Weiner, O. Bar-Am, S. Epsztejn, Z.I. Cabantchik, A. Warshawsky, M.B.H. Youdim, M. Fridkin, Bioorg Med Chem. 13 (2005) 773–783.
[11] H. Zheng, M.B.H. Youdim, M. Fridkin, J. Med, Chem. 52 (2009) 4095–4098.
[12] P.A. Adlard, A.I. Bush, J. Alzheimers Dis. 62 (2018) 1369–1379.
[13] W. Huang, W. Wei, Z. Shen, RSC Adv. 4 (2014) 52088–52099.
[14] K. Kaur, M. Jain, R.P. Reddy, R. Jain, Eur J Med Chem. 45 (2010) 3245–3264.
[15] (a). M. Di Vaira, C. Bazzicalupi, P. Orioli, L. Messori, B. Bruni, P. Zatta, Inorg Chem. 43 (2004) 3795–3797;
(b) M. Wehbe, A.K. Malhotra, M. Anantha, C. Lo, W.H. Dragowska, N. Dos Santos, M.B. Bally, Drug Deliv Transl Re. 8 (2018) 239–251;
(c) C.W. Ritchie, A.I. Bush, A. Mackinnon, S. Macfarlane, M. Mastwyk, L. MacGregor, L. Kiers, R. Cherny, Q.X. Li, A. Tammer, D. Carrington, C. Mavros, I. Volitakis, M. Xilinas, D. Ames, S. Davis, K. Beyreuther, R.E. Tanzi, C.L. Masters, Arch. Neurol. 60 (2003) 1685–1691.
[16] (a) L. Nguyen, J. Vendier, B. Stigliani, Meunier and A. Robert, Eur J, Inorg Chem. 2017 (2017) 600–608;
(b) L. Lannfelt, K. Blennow, H. Zetterberg, S. Batsman, D. Ames, J. Harrison, C.L. Masters, S. Targum, A.I. Bush, R. Murdoch, J. Wilson, C.W. Ritchie, Lancet Neurol. 7 (2008) 779–786.
[17] L. Lannfelt, K. Blennow, H. Zetterberg, S. Batsman, D. Ames, J. Harrison, C.W. Ritchie, Lancet Neurol. 7 (2008) 779–786.
[18] V. Guérineau, M. Rollet, S. Viel, B. Lepoittevin, L. Costa, P. Saint-Aguet, R. Laurent, P. Roger, D. Gigmes, C. Martini, V. Huc, Nat Commun. 10 (2019) 113.
[19] (a) S. Kimura, A. Kiriyama, K. Araki, M. Yoshizumi, D. Inoue, T. Furubayashi, R. Yutani, R. Teraoka, A. Tanaka, K. Kusamori, H. Katsumi, A. Yamamoto, K. Iga, T. Sakane, Eur J Pharm Biopharm. 122 (2018) 1–5;
(b) Y. Chong, Org. Biomol. Chem. 13 (2015) 11194–11199.
[20] A.N. Butkevich, G.Y. Mitronova, S.C. Sidenstein, J.L. Klocke, D. Kamin, D.N.H. Meineke, E. D'Este, P. Kraemer, J.G. Danzl, V.N. Belov, S.W. Hell, Angew Chemie Int Edit. 128 (2016) 3350–3355.
[21] D. Ren, Y. Liu, X. Liu, Z. Li, H. Li, X. Yang, Sens. Actuators B. 255 (2018) 2321–2328.
[22] X. Ma, J. Wang, Q. Shan, Z. Tan, G. Wei, D. Wei, Y. Du, Org. Lett. 14 (2012) 820.
[23] A. Gaeta, R.C. Hider, Brit. J. Pharmacol. 146 (2005) 1041–1059.
[24] A.I. Bush, Neurobiol Aging. 23 (2002) 1031–1038.
[25] J. Yang, Z.-L. Yuan, G.-Q. Yu, S.-L. He, Q.-H. Hu, Q. Wu, B. Jiang, G. Wei, J. Fluoresc. 26 (2016) 43–51.
[26] R.S. Juang, L.D. Shiau, Ind Eng Chem Res. 37 (1998) 555–560.
[27] S. Miah, I.M.M. Rahman, M. Takemura, S. Fukiage, A.S. Mashio, T. Maki, H. Hasegawa, Talanta. 194 (2019) 980–990.
[28] A. Fulgenzi, M.E. Ferrero, Int J Mol Sci. 20 (2019) 1019.
[29] Z.B. Zhao, H.X. Zheng, Y.G. Wei, J. Liu, Chinese, Chem Lett. 18 (2007) 639–642.
[30] G. Verreck, A. Decorte, K. Heymans, J. Adriaensen, D. Liu, D. Tomasko, A. Arien, J. Peeters, G. Van den Mooter, M.E. Brewster, Int J Pharm. 327 (2006) 45–50.
[31] V. André, O. Shemchuk, F. Grepioni, D. Braga, M.T. Duarte, Cryst Growth Des. 17 (2017) 6417–6425.
[32] M.A. Bailey, M.J. Ingram, D.P. Naughton, K.J. Rutt, H.T. Dodd, Transit Metal Chem. 33 (2008) 195–202.
[33] A. Goyanes, A.B.M. Buanz, G.B. Hatton, S. Gaisford, A.W. Basit, Eur J Pharm Biopharm. 89 (2015) 157–162.
[34] N. Oturan, C.T. Aravindakumar, H. Olvera-Vargas, M.M. Sunil Paul, M.A. Oturan, Environ Sci Pollut R. 25 (2018) 20363–20373.
[35] S.M. Bouzzine, S. Bouzakraoui, M. Bouachrine, M. Hamidi, J. Mol. Struc-Theochem. 726 (2005) 271–276.
[36] H. Derouiche, V. Djara, Sol Energ Mat Sol C. 91 (2007) 1163–1167.
[37] G.V. Loukova, V.P. Vasiliev, A.A. Milov, V.A. Smirnov, V.I. Minkin, J Photoch Photobio A. 327 (2016) 6–14.
[38] A. Paul, S. Anbu, G. Sharma, M.L. Kuznetsov, M.F.C. Guedes Da Silva, B. Koch, A.J.L. Pombeiro, Dalton Trans. 44 (2015) 16953–16964.
[39] Q. Dai, H. Liu, C. Gao, W. Li, C. Zhu, C. Lin, Y. Tan, Z. Yuan, Y. Jiang, New. J. Chem. 46 (2018) 613–618.
[40] S.K. Sahoo, D. Sharma, R.K. Bera, G. Crisponic, J.F. Callan, Chem. Soc. Rev. 41 (2012) 7195.
[41] (a). H. Irving, R.J.P. Williams, Nature 162 (1948) 746;
(b) H. Irving, R.J.P. Williams, Journal of the Chemical Society (Resumed). 637 (1953) 3192–3210.

[42] R. Englman, J.D. Dow, Phys Today. 27 (1974) 57.
[43] S. Liu, Y.M. Wang, J. Han, J. Photoch. Photobio. C. 32 (2017) 78–103.
[44] M. Formica, V. Fusi, L. Giorgi, M. Micheloni, Coord Chem Rev. 256 (2012) 170–192.
[45] H. Lineweaver, D. Burk, J. Am. Chem. Soc. 56 (1934) 658–666.
[46] Y. Zhao, X.B. Zhang, Z.X. Han, L. Qiao, C.Y. Li, L.X. Jian, G.L. Shen, R.Q. Yu, Anal. Chem. 81 (2009) 7022–7030.
[47] W. Cao, X.J. Zheng, C. Feng, L.P. Jin, Dalton Trans. 44 (2015) 5191–5196.
[48] T. Anand, G. Sivaramana, M. Iniya, A. Siva, D. Chellappa, Anal. Chim. Acta. 876 (2015) 1–8.
[49] F. Hou, L. Huang, P. Xi, J. Cheng, X. Zhao, G. Xie, Y. Shi, F. Cheng, X. Yao, D. Bai, Z. Zeng, Inorg Chem. 51 (2012) 2454–2460.
[50] M. Biancalana, S. K. Biochimica. BBA-Proteins. Proteom. 1804 (2010) 1405–1412.
[51] J.H. Viles, Coordin Chem Rev. 256 (2012) 2271–2284.
[52] E. House, J. Collingwood, A. Khan, O. Korchazkina, G. Berthon, C. Exley, J. Alzheimers Dis. 6 (2004) 291–301.
[53] (a) W. Garzon-Rodriguez, A.K. Yatsimirsky, C.G. Glabe, Bioorg Med Chem Lett. 9 (1999) 2243–2248;
(b) L.Q. Hatcher, L. Hong, W.D. Bush, T. Carducci, J.D. Simon, J. Phys Chem B. 112 (2008) 8160–8164;
(c) B. Alies, E. Renaglia, M. Rozga, W. Bal, P. Faller, Anal Chem 85 (3) (2013) 1501–1508;
(d) K.P. Kepp, Coordin. Chem. Rev. 351 (2017) 127–159.
[54] E. Gazit, Faseb. J. 16 (2002) 77–83.
[55] (a) L. Zhu, Y. Han, C. He, X. Huang, Y. Wang, J. Phys Chem B 118 (2014) 9298–9305;
(b) K. Murakami, T. Yoshioka, S. Horii, M. Hanaki, S. Midorikawa, S. Taniwaki, H. Gunji, K. Akagi, T. Kawase, K. Hirose, K. Irie, Chem Commun. 54 (2018) 6272–6275.